In **Advances in motor learning and control,** H.N. Zelaznik (Ed.). Champaign, IL: Human Kinetics Press, 1996.

Chapter 10

Neural Network Modeling of Sensory-Motor Control in Animals

Daniel Bullock, Stephen Grossberg, and Frank Guenther
Boston University

Neural network research spans many fields, including studies of vision, speech perception and production, reinforcement learning, memory, pattern recognition, and movement control. Within each of these areas, neural network researchers use many approaches to accomplish many goals. The purpose of this chapter is to introduce that subset of neural network modeling that seeks to understand the computations and neurophysiological bases of movement control in animals. To understand where this approach fits in with other approaches to using neural networks for control, as well as with other approaches in psychology, it will be useful to consider three potential goals of movement control studies:

1. Detailed characterization of the input-output functions of animal and/or human behavior or inferred components of such behavior
2. Detailed characterization of the anatomy and physiology of biological sensory-motor control
3. Technological applicability of the system

Many neural network researchers studying movement control are primarily interested in technological applicability, while only loosely pursuing goals 1 and 2. Much of the utility of neural networks in this research derives from their ability to learn complex nonlinear mappings. Examples of this approach can be found in Barto (1990), Jordan (1988), Kuperstein (1988), Miller (1987), Narendra (1990), and Ritter, Martinetz, and Schulten (1989). To the extent that biological systems are better at a task than current technology, these researchers attempt to mimic their performance. However, they make little attempt to account for details of animal performance not necessary for technological applications. Furthermore, the networks used in this approach show only a superficial resemblance to neurophysiology. The networks are massively parallel and composed of neuron-like units, but little or no attempt is made to relate the processing units to particular neural populations existing *in vivo*.

Traditional cognitive psychology, on the other hand, focuses on goal 1 with little concern for detailed characterization of the anatomical loci of model components and with almost no concern for technological applicability. Connectionist modeling (e.g., McClelland and Rumelhart 1981) represents a partial departure from this tradition by using neuron-like elements and massive parallelism. Like the engineering

approach just described, the resemblance to neurophysiology is only superficial, and comparison to specific neural populations is rarely carried out.

By contrast, the approach exemplified in the following sections strongly emphasizes goals 1 and 2 and places tertiary emphasis on goal 3. Proponents of this approach attempt to "open up the black box" (i.e., to build a model of the biological system that captures its constituent structure and the elementary functions describing interactions among the constituents—neural populations or subsystems). This is done by explaining not only psychophysical data, but also by using anatomical and neurophysiological data to constrain the model. Unlike connectionist approaches, the resulting model has a necessarily nonhomogenous structure that reflects the task specificity of neural circuitry; brain regions that perform different tasks have evolved both phylogenetically and ontogenetically to use different structure and connectivity. An accurate model computes the overall input-output function as a composition of these distinct, more elementary functions. This research strategy adheres to the slogan of the Swiss structuralist Piaget, that to understand is to reconstruct. The description of the constituent structure taken with the local laws of interaction provide an understanding of the mechanisms by which the aggregate input-output function is generated *in vivo*.

Examples of this approach can be found in Calabrese, Angstadt, and Arbas (1989), Grossberg and Kuperstein (1986, 1989), Houk and Gibson (1987), Ito (1984), Kawato, Furukawa, and Suzuki (1987), and Selverston and Moulins (1986). These models differ in the scope of the sensory-motor problems they address and the detail with which they describe the neural mechanisms involved. The remainder of this chapter describes a collection of interrelated neural models that cover a wide range of the field of neural networks for biological sensory-motor control. Readers unfamiliar with neural network models may at this point benefit from reading the appendix, which reviews elementary concepts in the analysis of neural networks as dynamical systems.

INTEGRATIVE EXAMPLE: REACHING TO A VISIBLE TARGET, OR HOW LIGHT GETS INTO THE MUSCLES[1]

One of the most studied tasks in the motor control literature is reaching to targets in space. Many neural network modelers have concentrated on a subset of the computations involved in the chain of events spanning from visually perceiving a target to issuing commands to the motoneurons involved in moving the arm to the target (e.g., Houk and Gibson 1987; Ito 1984; Zipser and Andersen 1988). Other researchers have attempted to model the entire task with simple network models (e.g., Kuperstein 1988; Ritter, Martinetz, and Schulten 1989; Gaudiano and Grossberg 1991). The remainder of this chapter reviews a research program concerned with describing this process in detail with a collection of neural network

[1]In the late 1970s, Michael Turvey often began his colloquia with the provocative question: "How does light get into the muscles?"

models that each perform a subtask in the larger task of visually guided reaching. Four networks, motivated by anatomical, physiological, and psychological data, collectively perform the following tasks:

- Neural representation of a visually perceived target within a head-centered coordinate frame
- Transformation of this representation into a body-centered coordinate frame
- Formation of a spatial trajectory from current hand position to the target
- Transformation of this spatial trajectory into joint angle commands (inverse kinematics)
- Invariant production of the commanded joint angle time courses despite large changes in muscle tension (inverse dynamics)

These models were formulated with strict attention to internal consistency; this includes several kinds of consistency within and between networks. First, because these networks are interconnected to form an integrated sensory-motor system, the representations used at the interfaces between the networks must be consistent. Second, because this collection of networks is formulated as a partial model of the human sensory-motor control system, the model must be consistent with motor control tasks other than reaching that will use many of the same subsystems. That is, the proposed solution for visually guided reaching should be constrained so the resulting model is compatible with the solution of other motor tasks such as handwriting. Third, because these networks are meant as mechanistic models of biological sensory-motor control, there must be consistency of model component types across networks, and consistency of these components with available neurophysiological data. The lowest-level components of these models correspond to neurons or populations of neurons, and many model cell types have been identified with neuron types *in vivo* whose properties closely match those of the model cells.

Strict attention is also paid to the role of learning within these models. Mechanical properties of biological systems change with time. For example, the lengths of arm segments and strengths of muscles change with age. To assure accurate reaching, parameter values in the sensory-motor control system (e.g., the weighting of synaptic connections) must be *adaptive*, not prewired at birth. However, performance of a reaching task under temporarily constraining conditions, such as blocked movement of a particular joint, should not require new learning to restructure the motor control system. Two later sections describe networks that generate the desired trajectories for reaches. These networks use information from an action-perception cycle in order to adaptively organize mappings that transform a head-centered representation of target positions into a body-centered representation, transform spatial movement commands into joint angle movement commands, and transform joint angle position information into spatial position information. The control system adaptively finds parameters that implicitly account for the relations among body segments and strengths of muscles, but do not use new learning to solve movement problems under temporary environmental constraints.

These networks were also formulated with attention to robust performance. The DIRECT model of trajectory formation and inverse kinematics, reviewed later, was motivated by motor equivalence data suggesting that humans can generate a spatial

movement trajectory in many ways, depending on environmental constraints. These data point to movement trajectory formation in spatial, rather than motor, coordinates, and this constrains the form of the head- and body-centered representations of space described in later sections. The DIRECT model provides robust performance of movement trajectories under conditions of visual shift, a blocked joint, or reaches with a tool, rather than the hand, as the end effector. The model performs these reaches automatically (i.e., without reverting to special performance modes and without requiring new learning under the different conditions). The FLETE network design, also described later, models spinal circuits that ensure the invariant production of commanded joint angle time courses in the face of conditions that lead to large variations in muscle tension.

To summarize, the collection of networks described in the following sections uses only information available in an ongoing action-perception cycle to learn the transformations necessary for an extremely flexible system capable of successfully performing several tasks under a variety of environmental conditions. Rather than optimizing performance for abstract criteria such as minimum jerk or minimum torque change (c.f. Flash and Hogan 1985; Uno, Kawato, and Suzuki 1987) by learning a set of model parameters specific to a single task, we believe that the optimization criterion of biological sensory-motor control systems is the rapid, successful performance of many motor tasks in a constantly changing environment.

FORMING A HEAD-CENTERED REPRESENTATION OF TARGET POSITION

The bilaterally symmetric organization of the body provides a simple and direct source of information for computing absolute position of a fixated target with respect to the observer's head and body. When both eyes binocularly fixate a target, the angle of intersection of the lines of gaze, which is a function of the eyes' attitudes in their orbits, may be used to compute the absolute distance and direction of the fixation point with respect to the head. Such extraretinal information may also be used to complement visual processing to derive better estimates of the absolute distance and direction of visually detected but nonfixated objects (see Grossberg et al. 1993).

Fig. 10.1 describes the geometry of three-dimensional target localization in terms of spherical coordinates that closely relate to the three-dimensional representation proposed here. The origin of this coordinate system, called the cranial egocenter, lies at the midpoint between the two eyes. Thus, the representation is *cyclopean*. The head-centered horizontal angle or azimuth, θ_H, and the vertical angle or elevation, ϕ_H, measure deviations from straight-ahead gaze. The radial distance R_H in the spherical coordinate frame of fig. 10.1 is replaced by vergence in the representations of three-dimensional space described herein.

Greve et al. (1993) and Guenther (1992) give evidence for such a coordinate system and a full description of a neural network model that forms a neural representation of target position based on this coordinate system. A less formal description of this network and the neurally generated representation follows.

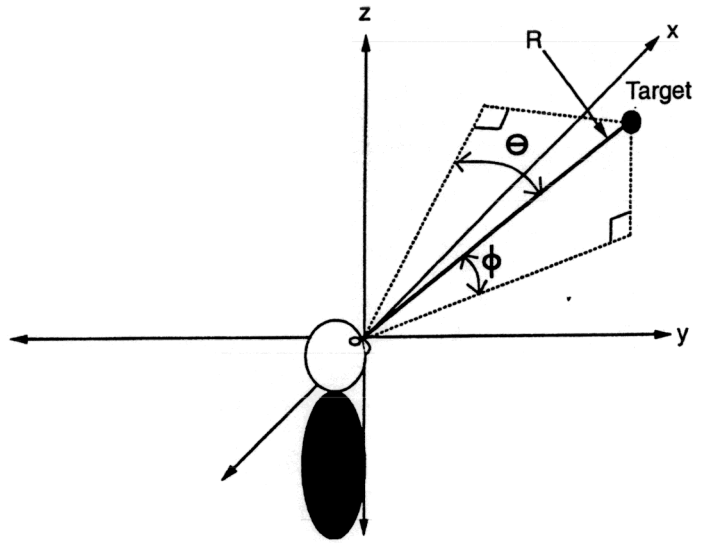

Fig. 10.1 Spherical coordinate frame for specifying a target position with respect to the head. This coordinate frame is related to the head-centered representation of space.

The head-centered representation neural network, shown in fig. 10.2, binocularly combines outflow signals from tonically active cells that control the position of each eye to form a head-centered representation of a foveated target. Forming such a representation is possible because the vector of command signals needed to orient two eyes to foveate a single point contains all the information needed to specify that point's three-dimensional location relative to the cranial egocenter. The extraction of this implicit information can be done in just two stages of opponent processing. First, opponent interactions combine the outputs of the cells that control the agonist and antagonist muscles of each eye. These opponent interactions give rise to opponent pairs of cells the sum of whose activity is approximately constant, or normalized (see Greve et al. 1993). The following equations define the resulting normalized internal representations of the horizontal angle of each eye:

$$l_1 + l_2 = \tag{10.1}$$

$$\theta_L = -90° + 180° \times l_2 \tag{10.2}$$

$$r_1 + r_2 = \tag{10.3}$$

$$\theta_R = -90° + 180° \times r_2 \tag{10.4}$$

where l_i indicates the activity of left eye cell population i, and r_i indicates the activity of right eye cell population i. Internal representations for the vertical angles of left and right eyes may be defined similarly. Thus

$$l_3 + l_4 = \tag{10.5}$$

$$\phi_L = -90° + 180° \times l_i \tag{10.6}$$

$$r_3 + r_4 = \tag{10.7}$$

$$\phi_R = -90° + 180° \times r_4. \tag{10.8}$$

Next, the normalized outputs from both eyes are combined in two ways to generate a head-centered spatial representation of the binocular fixation point. In particular, opponent cells from each eye generate inputs of opposite sign (excitatory and inhibitory) to their target cells at the next processing stage. As illustrated in fig. 10.2, one combination gives rise to a cell population whose activity h_2 approximates the angular spherical coordinate θ_H. The other combination gives rise to a cell population whose activity h_5 approximates the binocular vergence γ, which can be used to estimate the radial distance R_H. The two combinations generate head-centered coordinates by computing a sum and a difference of the normalized opponent inputs

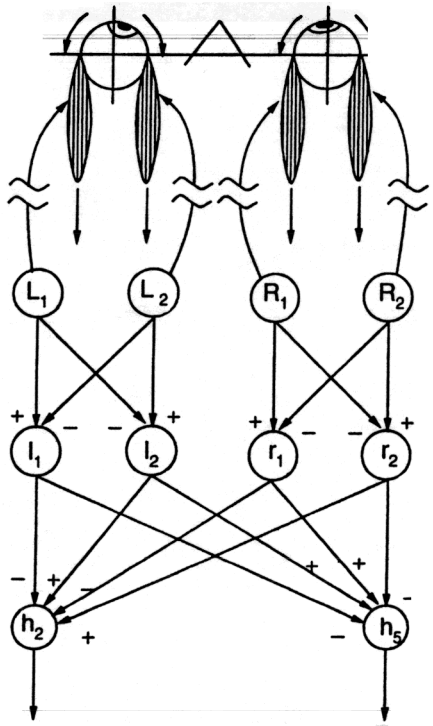

Fig. 10.2 Network for combining corollary discharges from both eyes, via two stages of opponent processing, into a head-centered representation of three-dimensional target position.

from both eyes. Such a general strategy for combining signals is well known in other neural systems, such as color vision. For example, a sum $L + M$ of signals from two color-vision channels estimates luminance, whereas a difference $L - M$ estimates color (DeValois and DeValois 1975; Mollon and Sharpe 1983). Thus, computations that may be used to control reaching in three-dimensional space are derived from a broadly used principle of neural computation. The following paragraphs describe the mathematical details of the combination of left and right eye muscle signals to produce a head-centered representation of space.

Let the cell populations h_i, $i = 1, 2, \ldots, 6$, form the basis for this head-centered spatial representation. These populations are arranged in antagonistic pairs. First we define cell activities h_1, h_2, h_3, and h_4 that linearly approximate the following estimates of θ_H and ϕ_H:

$$h_1 + h_2 = 1 \tag{10.9}$$

$$\theta_H = -90° + 180° \times h_2 \tag{10.10}$$

$$h_3 + h_4 = \tag{10.11}$$

$$\phi_H = -90° + 180° \times h_4 \tag{10.12}$$

These head-centered binocular representations of θ_H and ϕ_H emerge by simply averaging the corresponding monocular components derived from the left and right eye muscle command corollary discharges using a shunting on-center off-surround network. Specifically,

$$\frac{d}{dt}h_2 = -Bh_2 + (1 - h_2)(l_2 + r_2) - h_2(l_1 + r_1), \tag{10.13}$$

where B is a non-negative decay rate. Solving this equation at equilibrium ($dh_2/dt = 0$) yields

$$h_2 = \frac{l_2 + r_2}{B + l_1 + r_1 + l_2 + r_2} \tag{10.14}$$

Since $l_1 + l_2 \cong 1$ and $r_1 + r_2 \cong 1$, choosing a near-zero decay parameter B, such that $0 < B << 1$, leads to the approximation:

$$h_2 \cong \frac{l_2 + r_2}{2} \tag{10.15}$$

Likewise,

$$h_1 \cong \frac{l_1 + r_1}{2}. \tag{10.16}$$

so that, by (15) and (16),

$$h_1 + h_2 \cong 1 \tag{10.17}$$

To see how opponent computation leads to a representation of target distance, note that vergence is equal to the difference between r_1 (the normalized outflow command to the medial rectus of the right eye) and l_1 (the normalized outflow command to the lateral rectus of the left eye). Define antagonistic cell populations with activities h_5 and h_6 for internal representation of vergence. Let h_5 receive excitatory inputs l_2 and r_1 from cells controlling the medial recti of both eyes and inhibitory inputs l_1 and r_2 from cells controlling the lateral recti of both eyes (fig. 10.2). Then its activity will be governed by

$$\frac{dh_5}{dt} = -Ch_5 + (1 - h_5)(r_1 + l_2) - (h_5 + D)(l_1 + r_2), \tag{10.18}$$

where C and D are both non-negative. Here C is the decay rate and $-D$ is the lower bound on cellular activity h_5. At equilibrium,

$$h_5 = \frac{r_1 + l_2 - Dl_1 - Dr_2}{C + r_1 + r_2 + l_1 + l_2} \tag{10.19}$$

Because $r_1 + r_2 =$ and $l_1 + l_2 = 1$, equation (19) can be rewritten as

$$h_5 = \frac{1 - D}{C + 2} + \frac{1 + D}{C + 2}(r_1 - l_1) \tag{10.20}$$

If $D = 1$ and $C = 0$, then

$$h_5 = r_1 - l_1. \tag{10.21}$$

In this case, which might be considered ideal, subjective vergence equals physical vergence. A small departure from this ideal would occur if C were near zero but positive, and if D were slightly less than unity (i.e., if $0 < C << 1$ and $0 << D < 1$). Then the slope $(1 + D)(C + 2)^{-1}$ of h_5 versus $r_1 - l_1$ is less than 1, and the intercept $(1 - D)(C + 2)^{-1}$ of the function is positive. Such values are biologically plausible and compatible with the Foley (1980) estimate from psychophysical data of the internal representation of target distance.

FORMING A BODY-CENTERED REPRESENTATION OF TARGET POSITION

This section addresses the formation of a body-centered representation of three-dimensional target positions using the head-centered representation described in the previous section, coupled with information concerning the head position with respect to the torso. This work is described in detail in Guenther et al. (1994) and Guenther (1992). The adaptive computational strategy embodied by this network uses signals generated automatically during the typical behavioral sequence associated with changes of visual fixation. In a typical episode

1. the representation of a novel, initially nonfoveal visual target wins an internal competition that determines the next target to be foveated, and a saccade is made to this target;
2. information regarding head-centered target location is combined with information about neck muscle states to yield a stored estimate of target location relative to the body;
3. neck muscles rotate the head (either randomly or to point the nose toward the target) while the eyes make a vestibular ocular reflex (VOR)-mediated counterrotation to ensure continued foveation during the head movement; and
4. during the head movement and ocular counterrotation, both internal representations of the target's location in head coordinates and internal representations of neck angles change while the stored representation of target position in body coordinates remains constant.

If the network that combines head-centered representation and neck angle information to yield an estimate of target location in body coordinates is well tuned, then its estimate will remain invariant during the head rotation and ocular counterrotation. If it is not well tuned, then a discrepancy will develop during the head rotation between this network's current estimate and the estimate stored before the head rotation. This discrepancy may then serve as an error signal capable of directing a learning process that improves the network's knowledge, stored in its synaptic weights, about how to combine neck angle and head coordinate signals to estimate target positions relative to the body. The stage that registers the discrepancy in our model is called a difference vector (DV) stage, because errors are registered on a component-by-component basis. The Vector Associative Map (VAM) of Gaudiano and Grossberg (1991) is a neural mechanism that carries out DV-based learning; the current network uses a variant of VAM learning. The learning process described for this transformation requires no teacher and combines mechanisms known to be separately available *in vivo*.

The body-centered representation approximates a spherical coordinate frame that is similar to the spherical coordinate frame of fig. 10.1. The relationship between the head-centered and body-centered spherical coordinate frames is shown in fig. 10.3. The origin of the body-centered system is the same as the origin of the head-centered system when the head is pointed straight ahead. The body-centered frame also uses the same three spherical coordinates as the head-centered system, denoted by (θ_B, ϕ_B, R_B) in the body-centered frame. When the head points straight ahead, the head-centered representation (θ_H, ϕ_H, R_H) is identical to the body-centered representation (θ_B, ϕ_B, R_B). When the head moves from straight ahead, however, the head-centered frame moves with the head while the body-centered frame remains stationary.

The choice of these coordinate frames results from an investigation of the physiology of the head-neck systems of humans and many other vertebrates. The biomechanics of the neck vertebrae favor rotations of the head around preferred axes (Vidal et al. 1988). Movements along one of these preferred axes correspond to changes in θ_N (i.e., side-to-side or horizontal movements), whereas movements along the other preferred axis correspond to changes in ϕ_N (i.e., vertical movements). Movements along other axes, for example tilting the head to one side, are much more

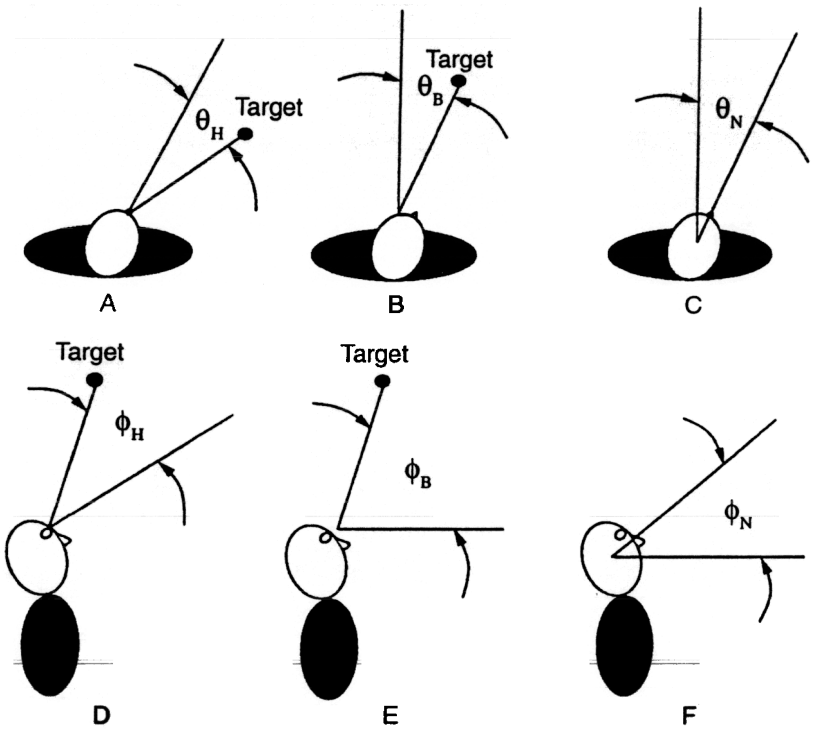

Fig. 10.3 Top view (*a, b, c*) and side view (*d, e, f*) showing relationships between the head-centered coordinates (*subscript H*), body-centered coordinates (*subscript B*), and head angles with respect to the body (*subscript N*).

constrained by the biomechanics of the neck. Further evidence for the biological importance of these preferred axes comes from Masino and Knudsen (1990), who showed that separate neural circuits controlled horizontal and vertical head movements in the barn owl.

The importance of these results in the current context is as follows. Learning to discount head movements in the body-centered representation consists of compensating for changes in head position by negating the resulting changes in the head-centered representation of a fixed target position. In other words, $(\theta_B, \phi_B) = (\theta_H, \phi_H) + (\theta_{correction}, \phi_{correction})$, where $(\theta_{correction}, \phi_{correction})$ is a learned correction based on neck muscle information. (The third coordinate in the two representations, distance from the head, changes little with head movement; see Guenther 1992, and Guenther et al. 1994, for further discussion of corrections to the vergence component.) When the transformation network is properly tuned, this correction is nearly linearly related, in fact nearly equal, to the head movement defined according to the preferred axes (i.e., θ_N, ϕ_N). This linear relation between head movements and the required correction to the head-centered representation allows very fast and accurate learning of the correction. The relationship between head movements and other head- and body-centered coordinate frames, such as Cartesian, is much more complex, making the

transformation from a head-centered representation to a body-centered representation far more difficult to learn.

Although head position (θ_N, ϕ_N) can be derived from neck muscle length information, an organism cannot, without learning, use this neck muscle information accurately to compensate for head movements when forming a body-centered representation. This is because the relationship between any neck muscle length and head position is dependent on details of the neck anatomy that vary from individual to individual and can change with time (e.g., growth). Therefore, the organism must *adaptively* find parameters that allow neck muscle length information to compensate for changes in head position. The network described in the following paragraphs rapidly and successfully finds these parameters without an external teacher. Instead, network construction capitalizes on the fact that the positions of fixed objects with respect to the body do not change while the head moves, allowing the organism to internally generate teaching signals. We briefly describe this process in the following paragraphs.

Fig. 10.4 illustrates the network used for the simulations. We omit populations corresponding to representations of R_H and R_B in this section due to the relative independence of these variables with respect to neck movements. In this network, there are five main neural population types:

1. Neck muscle length populations with activities n_{ij} $(1 \le i \le 9,\ 1 \le j \le 2)$
2. Head coordinate representation populations with activities h_i $(1 \le i \le 4)$
3. Head-neck Difference Vector (DV) populations with activities x_i $(1 \le i \le 4)$
4. Unnormalized body coordinate representation populations with activities $b_i^{(1)}$ $(1 \le i \le 4)$
5. Normalized body coordinate representation populations with activities $b_i^{(2)}$ $(1 \le i \le 4)$

Each head-centered representation population projects with a fixed-weight connection to the corresponding DV population. Each neck muscle length population projects to every DV population through an adaptable-weight synaptic connection, indicated by filled semicircles in fig. 10.4. Furthermore, VOR-mediated gating modulates the interactions between the DV populations and the unnormalized body-centered representation populations. The learning law in the simulations is as follows:

$$\frac{d[z_{ijk}]}{dt} = -\varepsilon x_k[-Ez_{ijk} + n_{ij}] \tag{10.22}$$

where z_{ijk} is the weight of the synaptic connection between neck muscle length activity n_{ij} and DV population activity x_k, ε is a learning rate parameter with a small positive value, and E is a decay rate parameter. Thus, learning is local (i.e., it depends only on the pre- and post-synaptic cell activities, not on activities or activity changes at distant points in the network).

The following steps were used to train the network:

1. Initialize all weights to 0.0.
2. Choose a random initial head position (θ_N, ϕ_N).
3. Choose a random target position (θ_T, ϕ_T).

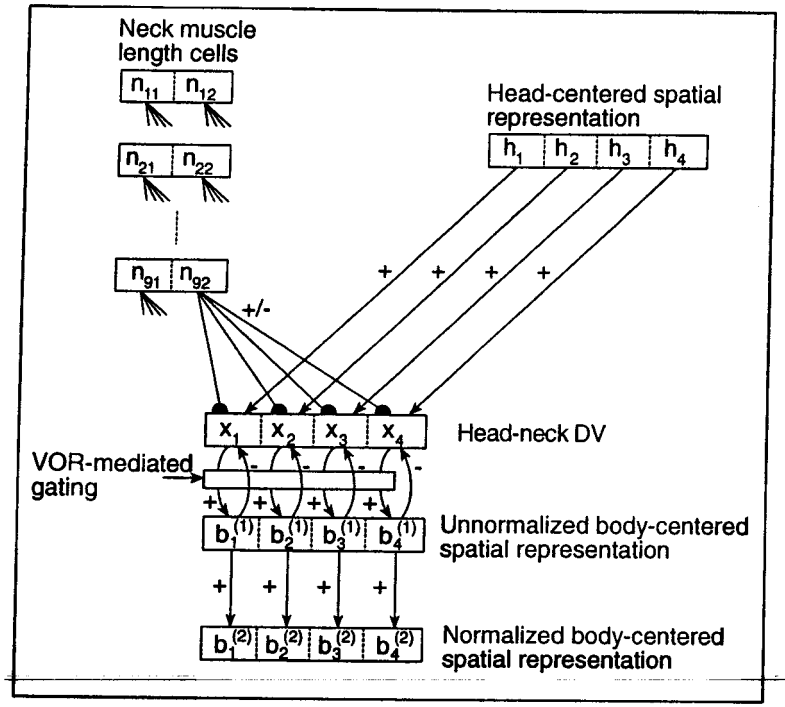

Fig. 10.4 Network for learning transformation from a head-centered spherical coordinate representation to a body-centered spherical coordinate representation of target position.

4. Foveate a new target (i.e., adjust h_i so that $\theta_H = \theta_T - \theta_N$ and $\phi_H = \phi_T - \phi_N$) and store this target into the body coordinate populations $b_i^{(1)}$ and $b_j^{(2)}$. This step corresponds to the breaking of VOR fixation to foveate and store a new target. Storing the target is presumed to be carried out by the transient opening of the gated excitatory pathways from the populations x_i to the populations $b_j^{(1)}$. This gating action is presumed to occur each time VOR fixation is broken.
5. Choose a new head position while remaining foveated on the current target (i.e., change n_{ij} and adjust h_i accordingly to keep $\theta_H + \theta_N = \theta_T$ and $\phi_H + \phi_N = \phi_T$). This step corresponds to moving the head while using VOR to keep the target foveated.
6. Adjust the weights from the neck muscle length populations to the head-neck DV populations according to equation (22).
7. If more trials remain, repeat steps 3 through 7.

Despite the use of simple, local learning laws and no external teacher, the system globally self-organizes to perform the required transformation from a head-centered to a body-centered representation of three-dimensional target positions. Fig. 10.5A shows the internal representation (left side) and actual target position (right side) during a head movement after 20 learning trials. As the head moves, the internal representation of the target position also moves, even though the actual target

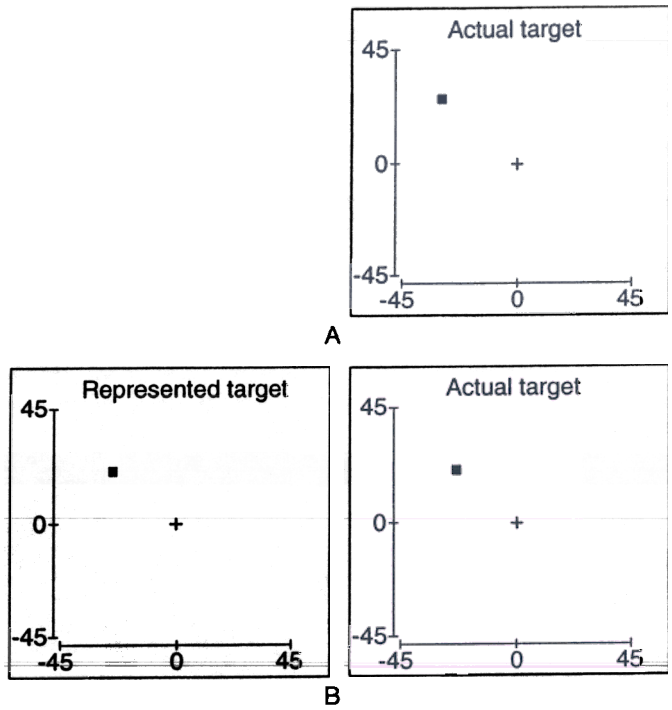

Fig. 10.5 (*A*) Results after 20 learning trials. The *left side* shows the internally represented body-centered target position as the head is moved through over 30° of both horizontal and vertical angle. The *right side* shows the actual target position. The change in represented target position as the head is moved indicates that the network has not yet learned to invariantly represent body-centered target position. (*B*) Results after 200 learning trials. The *left side* shows the internally represented body-centered target position as the head is moved through over 30° of both horizontal and vertical angle. The *right side* shows the actual target position. The internal representation is now invariant under head movements.

position with respect to the body remains fixed. After foveating only 200 targets, however, the network has learned to invariantly represent the body-centered target position despite large head movements, as shown in fig. 10.5B.

DIRECT: TRAJECTORY FORMATION AND INVERSE KINEMATICS

Once the position of a target relative to the body is known, a trajectory from the current hand position to the target must be formed. The phenomenon of motor equivalence (i.e., the ability to realize a movement goal using motor means that vary from trial to trial) implies that trajectory formation is controlled in spatial, rather than motor, coordinates. For example, it is well known that the overall spatial

shape of written letters remains remarkably consistent when produced with entirely different effector systems (Merton 1972; Raibert 1977). Spatial trajectory formation is also supported by psychophysical data, which show that the spatial characteristics of movements to targets remain invariant across movements despite large variations in the joint angle characteristics from movement to movement (e.g., Morasso 1981) or changes in the end effector used to reach to the target (e.g., Lacquaniti, Soechting, and Terzuolo 1982). The ability to produce a desired movement trajectory in many ways results in robustness of movement performance under a variety of environmental conditions.

The representation of target positions described earlier is consistent with trajectory formation in spatial coordinates. The Vector Integration to Endpoint (VITE) model (Bullock and Grossberg 1988a, 1991) is a neural network model of trajectory formation that exhibits key kinematic properties of human movements, including asymmetric bell-shaped velocity profiles (e.g., Nagasaki 1989; Zelaznik, Schmidt, and Gielen 1986). As shown in fig. 10.6, this model has three stages, each of which computes a vector much like the body-centered representation (b_1, b_2, . . . , b_6): a target position vector (*TPV*), which specifies the desired joint angles that define the end goal of a movement, a present position vector (*PPV*), which specifies the current joint angles, and a difference or direction vector (*DV*) formed by subtracting the *PPV* from the *TPV*. The *DV* thus specifies the desired movement direction and magnitude. In the VITE model, it is fundamental that the *DV* be computed before movement and stored until movement initiation. This precomputation and storage is called motor priming, an important precursor of deliberate action and fully voluntary movement (Busemeyer and Townsend 1993; DeJong et al. 1990). The phenomenon of voluntary release of a primed movement implies that there must be an internal signal whose activation allows the *DV* to be expressed. This signal is called the *GO* signal, and its action is analogous to opening a gate between the primed *DV* and the effector apparatus. Closing and opening of this gate is captured in the model

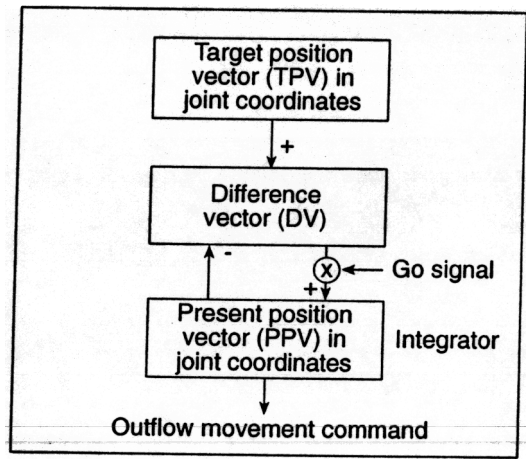

Fig. 10.6 Block diagram of the VITE model

by assuming that the *GO* signal is zero during the priming interval but positive during movement, and that *GO* multiplies the *DV* before the latter affects the effector apparatus via the *PPV* stage. Then $DV \times GO$ specifies desired movement velocity, and making *GO* positive serves the dual function of releasing movement and scaling its speed. If the $DV \times GO$ signal is integrated at the *PPV* stage, a process we call *PPV* updating, then the *PPV* moves toward the *TPV* after *GO* becomes positive, and the *PPV* specifies desired position in joint coordinates.

Taken together, $DV \times GO$ and *PPV* give the desired movement trajectory, which evolves gradually. Because of the inhibitory feedback from the *PPV* to the *DV* stage, the *DV* is driven to zero by *PPV* updating. When *PPV* reaches *TPV*, $DV = 0$. Therefore, $DV \times GO = 0$ even if *GO* remains large, and the movement self-terminates at the target coordinates. If the onset of *GO* is gradual, such that *GO* exhibits growth through much of the movement time, then velocity profiles have the smooth, bell-like form characteristic of human and animal movement.

However, VITE falls short as a comprehensive model of movement control—even for elementary visually guided movements. It does not explain how to compute the *TPV* in joint coordinates assumed by the model. Thus, it does not solve the inverse kinematics problem: how can a goal specified in three-dimensional spatial coordinates be realized by movements involving changes in joint coordinates, which may have many more than three dimensions? As noted earlier, the conservation of spatial form across movements made with varying effectors (the motor equivalence phenomenon) suggests that three-dimensional spatial computations are a critical aspect of the process of trajectory formation. The **DI**rection-to-**R**otation **E**ffector **C**ontrol **T**ransform (DIRECT) model (Bullock, Grossberg, and Guenther 1993; Guenther 1992), schematized in fig. 10.7, extends the VITE model to allow spatial trajectory formation with motor equivalent movement production. The motor coordinates *TPV* and *PPV* of VITE are replaced by a spatial target position vector (TPV_s) and spatial present position vector (PPV_s). The PPV_s is then subtracted from the TPV_s to form a difference vector (DV_s), which represents the desired movement magnitude and direction in spatial coordinates.

Once this desired movement direction has been formulated, the problem of mapping into motor coordinates to control the joint angles, or the inverse kinematics problem, must still be solved. The DIRECT model learns a solution, which transforms DV_s into a motor direction vector (DV_m) specifying joint rotations. This transformation from directions in three-dimensional space into joint rotations plays a key role in producing motor equivalent reaching (see Bullock, Grossberg, and Guenther 1993). The DV_m components are then integrated by a motor present position vector (PPV_m) that specifies commanded joint angles. As in VITE, signals from the DV_m to the PPV_m stage can be gated by a *GO* signal.

The DIRECT model contains two learned transformations, indicated by filled semicircles in fig. 10.7: the spatial-to-motor transformation, which commands the motor actions needed to carry out a spatially defined trajectory, and a motor-to-spatial transformation, which allows motor information regarding end effector position to be used in place of visual information when performing reaches without visual feedback. As in the previous networks, learning in the DIRECT model is achieved through autonomously generated repetition of an action-perception cycle, which generates the associative information needed to learn these transforms. Piaget

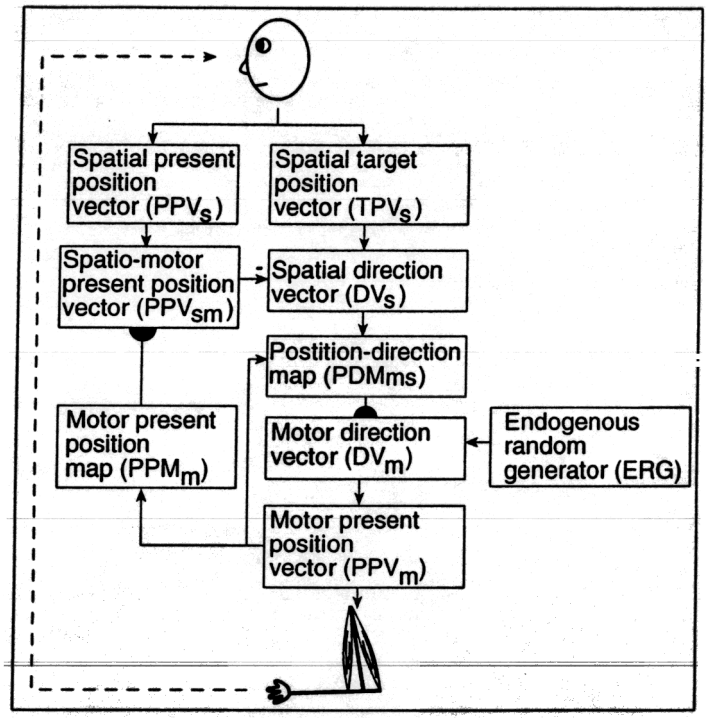

Fig. 10.7 Block diagram of the DIRECT model

(1963) called this cycle a *circular reaction*. A circular reaction endogenously creates movements in babies during a *motor babbling* phase, and leads to learning transformations among representations correlated through these movements. After learning takes place, the movements may be carried out in an intentional, or goal-oriented, manner.

Motor babbling is energized by an Endogenous Random Generator, or ERG, whose activations are integrated to generate movement commands (Gaudiano and Grossberg 1991). In the DIRECT model, ERG activations excite the DV_m stage, which encodes motor commands for rotating the joints, causing spontaneous arm movements during the motor babbling stage. The network uses the information generated by these spontaneous arm movements in several ways. Visual feedback provides information about the positions and directions of movements in three-dimensional space. Internal feedback provides information about the joint configurations that generate these movements. The network is designed to combine these multiple sources of information in a manner that solves the motor equivalence problem.

During motor babbling, the endogenously moving end effector is a salient visual target. As the system visually tracks its own end effector, information regarding the direction of end effector movement, represented at the DV_s stage during motor babbling, drives learning of the spatial-to-motor transformation. To convert DV_s

activations into effective reaching behaviors, each DV_s must be transformed into a DV_m, which produces movement in the corresponding spatial direction; that is, spatial directions need to be converted into joint rotations. The appropriate DV_m to learn depends on the configuration of the arm when the DV_s is computed. The conjoint activation of the PDM_{ms} stage by both the PPV_m stage and the DV_s stage activates a few cells in the PDM_{ms} map. Topographic maps such as the PDM_{ms} are found in many areas in the brain, and self-organizing neural networks that form such maps have been extensively studied (e.g., von der Malsburg 1973; Grossberg and Kuperstein 1986, 1989; Kohonen 1984). This map architecture allows the PDM_{ms} cells to learn the babbled DV_m activity that is producing the motion direction registered at the DV_s stage. Learning takes the form of a local, Hebbian learning law with gated decay called the *outstar* learning law (Grossberg 1968, 1982; Levine 1991).

A motor-to-spatial transformation is also learned during motor babbling. The goal of this transformation is to convert a motor representation PPV_m of the present end effector position into a visual representation (i.e., in the same coordinate frame as PPV_s) of present end effector position. The vector representation PPV_m is transformed into a map representation PPM_m via a self-organizing feature map, and the PPM_m cells learn corresponding PPV_s vectors at the PPV_{sm} stage via outstar learning. In this way, a configuration coded at the PPV_m stage learns to predict the corresponding spatial position of the end effector as represented through vision at PPV_s.

In summary, during motor babbling, the *ERG* spontaneously generates motor vectors DV_m that are integrated into arm movements by the PPV_m stage. The arm movements draw visual attention to the end effector. As a result, spatial DV_s vectors are computed that, conjointly with PPV_m feedback signals, enable the PDM_{sm} map to learn an appropriate DV_m with which to move in the corresponding spatial direction DV_s when the end effector is at PPV_m. Simultaneously, joint configurations coded by the PPM_m stage are associated through learning at the PPV_{ms} stage with the corresponding spatial positions PPV_s of the end effector perceived through vision.

These movements and learning events during motor babbling are not goal oriented. The babbled movements are endogenously activated, and the learning events correlate spatial and motor representations coactivated by the babbled movements. During subsequent goal-oriented reaching movements, the target is not typically the end effector, so the information coded at TPV_s and at PPV_s is not the same. The DIRECT model is designed such that, after motor babbling ends, when a target other than the end effector activates TPV_s, the difference between present position of the end effector at PPV_{sm} and the target position at TPV_s is computed at DV_s, and the arm is steered toward the target by activating an appropriate series of DV_m vectors to move the arm in the desired direction. If visual feedback of the end effector is not available during the reach, then the motor pathway $PPV_m \rightarrow PPM_m \rightarrow PPV_{sm}$ is used to estimate end effector position, rather than the visual pathway $PPV_s \rightarrow PPV_{sm}$. In particular, after learning, the DIRECT model uses gating signals to direct the flow of visual information to the PPV_s block if the visually attended spatial position corresponds to the end effector, or to the TPV_s block if the visually attended spatial position corresponds to a goal-oriented movement target. This requires the developing system to incorporate some mechanism for differentiating between self-generated movements of the hand and other potential targets of visual attention (moving or stationary) in the visual field. For a thorough discussion of these gating signals and

a possible mechanism for providing this self versus other distinction, see Guenther (1992).

DIRECT model simulations of a three-joint arm performing reaches in two-dimensional space verify the model's performance of unconstrained reaches to targets, reaches with one joint blocked during the reach, reaches using a tool or pointer as the end effector, reaches with visual input shifted by 30°, and reaches with no visual feedback of end effector position during the reach. It is important to note that training was done only in normal mode (i.e., with no blocked joints, no tools, and no shifted visual input). Yet because of the direction-to-rotation inverse kinematic mapping, the model automatically compensates for these different conditions to perform the reach successfully on the first try. Fig. 10.8 shows the model performing reaches using a tool as the end effector. The target is the small box at the end of the effector, and the tool is the fourth segment of the effector projecting from the box at the hand to the target. By simply representing tool tip position rather than hand position at the *PPV*, block (corresponding to visually attending to the tool tip during the reach), the model automatically produces accurate reaches with this novel fourth effector segment of arbitrary length and angle with respect to the hand.

As with the networks reviewed earlier, the DIRECT model components correspond to neurons or populations of neurons, and synaptic learning uses only information available at the pre- and post-synaptic cells. Because of this, the DIRECT model

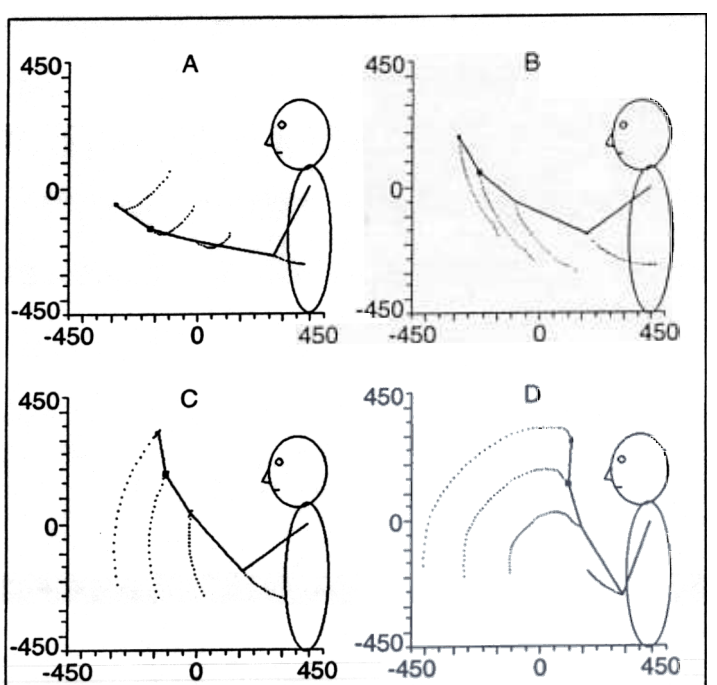

Fig. 10.8 Trajectories formed by the model using a pointer for reaching

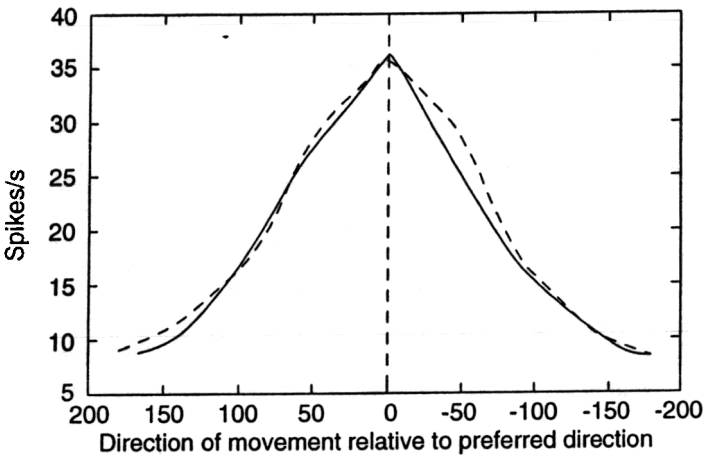

Fig. 10.9 Directional tuning curve averaged over 500 measurements of the joint velocity cells in different parts of joint space for the simulated model (*solid line*) and corresponding data from Kalaska et al. (1989) (*broken line*). Model data has been scaled to cover the same range as the Kalaska et al. data.

may provide insights regarding neurophysiological data. Many neurophysiologists have reported that motor cortical cells seem to be broadly tuned to desired direction of movement (e.g., Georgopoulos et al. 1982; Kalaska et al. 1989). That is, a motor cortical cell fires with maximal response rate for movement in a preferred direction, and at progressively lower rates for movement directions farther from the preferred direction. Fig. 10.9 compares the averaged tuning curve of the DIRECT model DV_m cells to neurophysiological data from the motor cortex. The solid line in fig. 10.9 indicates the average form of DV_m tuning curves in the model after training. The broken line in fig. 10.9 shows an averaged tuning curve obtained from single cell measurements in primate motor cortex by Kalaska et al. (1989). Based on the similarities in these curves and several additional comparisons, including the time course of real cell and model cell activities during movement, we believe that the DIRECT model provides insights about how and why these tuning curves might arise in motor cortical cells.

Ideas from the VITE and DIRECT models have recently been used to model behavior with serial structure. In particular, the DIVA model of Guenther (1992, 1994) treats speech production, whereas the VITEWRITE model of Bullock, Grossberg, and Mannes (1993) treats handwriting production. Both treatments demonstrate that we can replace many older ideas about stored motor programs once we recognize that movement properties can be better understood as emergent characteristics of adaptive dynamical systems.

FLETE: ACCURATE REACHING DESPITE VARIATIONS IN TENSION

The networks described so far give an account of the transformations from visual localization of a target to issuing joint angle commands that move the arm to the

target. However, successful performance of these joint angle commands requires the answer to many questions that fall under the heading of inverse dynamics, or how to generate the forces needed to realize kinematic goals. How can a limb be rotated to, and stabilized at, a desired angle? How can joint stiffness be varied independently of joint angle? How can the movement speed from an initial to a desired final angle be controlled under conditions of low joint stiffness? How can launching and braking forces be generated to compensate for inertial loads? Simultaneous achievement of these abilities requires a complex neuromuscular system, with several identifiable subsystems.

These tasks require that each muscle be able to generate a wide range of tensions at any length it may assume as the limb (into which it inserts) rotates. More stringently, these tasks require **F**actorization, or independent control, of muscle **LE**ngth and muscle **TE**nsion. This overarching theme led to the acronym "FLETE" for an original mathematical model of the neuromuscular system described in Bullock and Grossberg (1988b, 1989). The components of the FLETE model will be briefly introduced here; see Bullock and Contreras-Vidal (1993) and Bullock, Contreras-Vidal, and Grossberg (1993b) for a complete description of the motivation for these components, their functionality, and simulation results verifying their contribution to model performance.

The first question we will address concerns how a limb can be rotated to, and stabilized at, a desired angle. Fig. 10.10A schematizes a system in which two opposing muscles insert into a distal limb segment connected by a rotary or hinge joint to a more proximal limb segment, similar to the human forearm's connection to the upper arm. Suppose such a forearm segment is initially at rest and that $F_1 = F_2$, where the F_i, $i = 1, 2$ denote the pulling forces exerted by the opponent muscles. Then the limb can be set in motion by making the forces F_1 and F_2 unequal. The limb can be halted and stabilized at a new joint angle if the forces re-equilibrate as it approaches that angle and if the system can automatically generate whatever new muscle force imbalance may be needed to return it to the desired angle after any deviation (e.g., after the rotating limb initially overshoots the desired angle).

As many observers have noted (Cooke 1980; Feldman 1986; Polit and Bizzi 1979), muscle itself seems to have evolved to help provide this basic functionality. Essentially, muscle is springy tissue with a neurally controllable contractile component, which gives it a neurally modifiable threshold length for force development (Rack and Westbury 1969). To highlight this essence, at risk of oversimplification,[2] we can assume that the force F_i developed by a muscle is a threshold-linear function of its length L_i, its fixed resting length Γ_i, its stiffness, k, and its neurally modifiable contractile state, C_i:

$$F_i = k[L_i - (\Gamma_i - C_i)]^+ \tag{10.23}$$

where notation $[w_i]^+$ means max $(0, \omega_i)$. So if $\omega_i = L_i - (\Gamma_i - C_i) > 0$, $F_i = k \cdot \omega_i$; if $\omega_i \leq 0$, $F_i = k \cdot 0 = 0$.

[2]A better approximation to real muscle, whose stiffness also varies with contractile state, is gotten by replacing (23) with $F_i = k \cdot g([L_i - (\Gamma_i - C_i)]^+)$, where $g(x)$ is nonlinear (e.g., quadratic). See Bullock and Contreras-Vidal (1993) for further treatment.

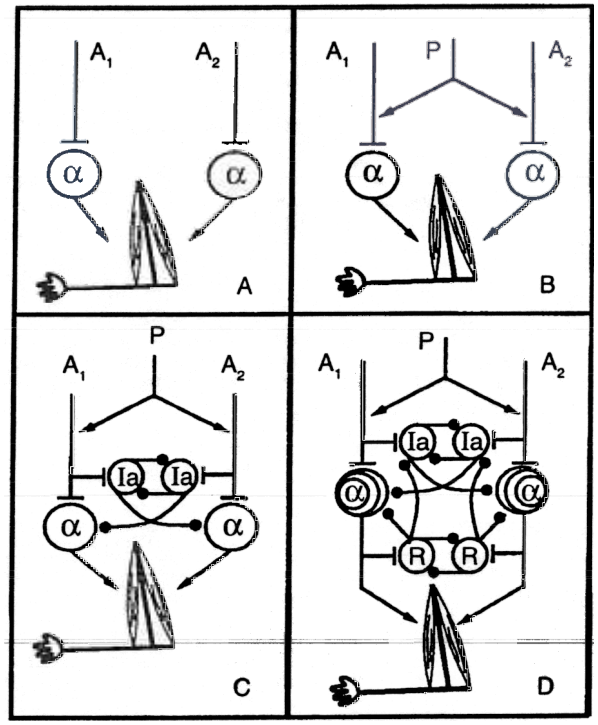

Fig. 10.10 Stages in the construction of the FLETE model. Excitatory connections are indicated by *flat bars*, inhibitory connections by *filled circles*. (*A*) Opponent alpha-motoneuron pools provide neural control over muscle contractile states and thereby the balance of forces acting across the joint. A motor intention can take the form of a pattern of descending signals (A_1, A_2) to the α-*MN* pools. (*B*) Joint stiffness can be controlled by adding descending signal P to both signals A_1 and A_2. The signal P is capable of producing high levels of co-contraction of the opponent muscles. (*C*) Design for alleviating saturative loss of sensitivity by α-*MN* pools to the difference $A_1 - A_2$ when signal P becomes large. The added model interneurons have the same connectivity as *Ia* interneurons known to exist *in vivo*. (*D*) Alpha-motoneurons have different sizes, which correspond to different thresholds for recruitment, and Renshaw cells "tap the cables" running from α-*MN* pools to muscles. Their negative feedback to α-*MN*s can compensate for distortion introduced by the size principle.

Equation (23) shows that a muscle is springlike in that it develops a force only when stretched to a length L_i greater than the effective threshold length, $\Gamma_i - C_i$. However, it also shows that muscle is more versatile than an ordinary spring, because this threshold can be neurally adjusted by varying the muscle's state of contraction, C_i.

To gain control over contractile states C_1 and C_2, there must exist (see fig. 10.10A) opposing alpha-motoneuron pools α-MN_1 and α-MN_2, whose axons project to, and allow differential activation of, the opposing muscles. Let the activation levels of

the opposing motoneuron pools be designated by M_1 and M_2. Then, as shown in fig. 10.10A, a motor intention—a neural state corresponding to specification of a desired joint angle—can take the form of a pattern of signals (A_1, A_2) suitable for inducing a differential pattern of activation (M_1, M_2) across the motoneuron pools. This creates a pattern (C_1, C_2) of contractile states, thereby creating a new stable point (L_1, L_2) for the limb. So if nothing goes wrong along the way, motor intention (A_1, A_2) will invariably lead to desired joint angle $\theta(L_1, L_2)$. We now show that many things can go wrong along the way, and all the circuitry that distinguishes fig. 10.11 from fig. 10.10A will be motivated by the animal's need to reduce errors of motor realization to a minimum.

Historically, analyses of what can go wrong in motor realization have focused on how nonmuscular forces imposed by the external world can complicate the story we kept simple by assuming that only muscular forces were acting on the limb. We now supplement such analyses by turning our attention inward, to neural, neuromuscular, and musculoskeletal sources of error variance.

Suppose that we want to improve on the fig. 10.10A system by adding the ability to stiffen a joint in varying degrees while holding joint angle constant. Such joint

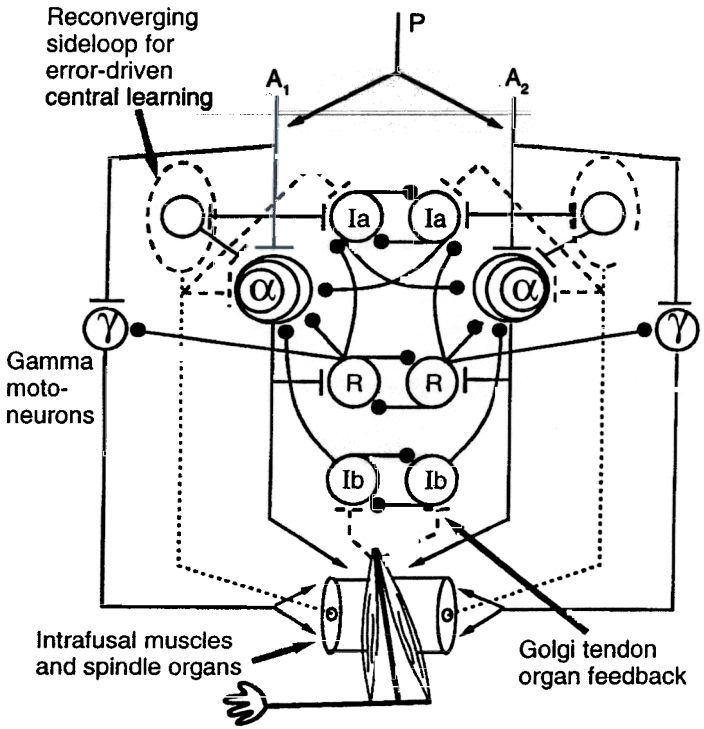

Fig. 10.11 The force feedback from Golgi tendon organs can compensate for muscle fatigue, and a parallel neuromuscular system comprising γ-*MN*s, intrafusal muscles, and spindle receptors allows measurement of residual positioning errors. Spindle feedback signals act locally via the stretch reflex, but also project to the higher brain, where they may guide recalibration of descending commands.

stiffening is known (e.g., Humphrey and Reed 1983) to involve simultaneous increments to the contractile states of the joint's opponent muscles, which results in co-contraction.

The simplest way for the higher nervous system to effect a co-contraction is to add a signal, whose magnitude we will denote by P, to both components of the signal pattern (A_1, A_2). Then the net input to the opponent α-MN_s would be $(A_1 + P, A_2 + P)$. This modification is shown in fig. 10.10B. If variations in P always have the same effect on muscle-force production in both opponent channels, then a limb initially at equilibrium at a desired angle θ will remain there as P varies: Though F_1 and F_2 will both increase or decrease, their difference will remain unchanged. Such an invariant relationship between (A_1, A_2) and θ under variations of co-contraction signal P can be summarized by

$$\theta(A_1, A_2) = \theta(A_1 + P, A_2 + P) \tag{10.24}$$

Threats to this desirable invariance property arise due to the property of physical neurons called *saturation*, or loss of sensitivity to input differences near the upper bound of neuronal activity. Grossberg (1973) noted decades ago that saturative loss of sensitivity to differences existing across pattern processing channels can be prevented by allowing the channels to interact laterally via inhibitory signals. *In vivo*, inhibitory interneurons called *IaIN*s are known to exist with the signed connectivity, vis-a-vis α-*MN*s and each other, shown in fig. 10.10C. Sherrington, in his experiments on the stretch reflex, demonstrated the need for a pathway to mediate reciprocal inhibition between opponent muscle channels. The *IaIN*s of fig. 10.10C are known to receive feedback from stretch receptors and from Renshaw cells (both of which we introduce into the model in later paragraphs). Our remarks on the computational necessity for *IaIN*s are compatible with, but also extend prior proposals regarding their function. In particular, we agree that for rapid movements to be energetically efficient, it is important to prevent an antagonist muscle from retarding the action of an agonist muscle. This would be difficult if the only process for lowering α-*MN* activation levels were a passive decay process, especially with the small passive decay rates seen *in vivo*. Reciprocal inhibition via *IaIN*s allows rapid decrementing of activity in antagonist alpha-motoneuronal pools.

We next need to ask whether the pattern (M_1, M_2) induced by motor intention $(A_1 + P, A_2 + P)$ is faithfully registered in the pattern (C_1, C_2) of contractile states induced by activities M_1, M_2. To see why it would not be, in the absence of further structure, consider a simple differential equation describing changes in contractile state through time:

$$\frac{d}{dt}C_i = (B_i - C_i)M_i - \delta C_i \tag{10.25}$$

This says that a sufficiently large neural input M_i can push contractile state C_i up to the limit B_i, and that contractile state relaxes at rate δ. *In vivo*, B_i corresponds to the maximal number of muscle fibers that can be simultaneously activated.

The presence of an upper bound B_i means that the ability of the C_i to remain sensitive to differences across the M_i can saturate if the range of M_i is too large relative to B_i. This problem can be avoided, given the neural provisions that avoid

M_i saturation in fig. 10.10C, if B_i is itself a function of M_i. In fact, this is assured *in vivo* by a motor unit design principle with a progressive recruitment rule. Motor units are composed of distinct alpha-motoneurons that project to distinct sets of contractile fibers. Moreover, within the motoneuron pools, there exist distributions of activation thresholds such that larger net excitatory inputs to the pool recruit larger numbers of motor units. Because smaller α-*MN*s are recruited earlier and larger later, this rule has been called the size principle of motoneuron recruitment (Henneman 1957). Fig. 10.10D schematizes the addition of a size principle to our model by showing a stacked series of α-*MN* cells with increasing diameter.

Unfortunately, introduction of the size principle by itself causes a loss of independent control of joint angle by (A_1, A_2) and of joint stiffness by signal P. To see this, note that under all initial choices of (A_1, A_2) other than $A_1 = A_2$, signal P will cause deeper recruitment in one muscle channel than the other. Because of the size principle, part of the signal P is subjected to greater amplification in that channel where recruitment is deeper, and a resultant force imbalance develops in that channel's favor. In consequence, the animal who had hoped to stabilize its limb at its initial posture by stiffening the joint would instead experience a large, unwanted, limb rotation!

Such an unequal amplification could be neurally compensated if it could be measured. Because the α-*MN*s, which are directly linked to muscle, are usually looked upon as the last stage of the nervous system, we might suppose that the unequal amplification could be measured only by its effect on muscle (e.g., by way of stretch receptors embedded in the opponent muscles). However, because muscle contraction is slow relative to the unequal neural amplification, a significant rotation error could develop before it could be halted by feedback from stretch receptors.

In fact, the α-*MN*s project directly to muscle and directly to a class of cells called Renshaw cells, whose function has not been well understood. In Bullock and Grossberg (1988b, 1989), we proposed that these Renshaw cells were perfectly situated to measure and to compensate for unequal amplifications of a co-contractive signal P sent to both opponent muscle channels. As shown in fig. 10.10D, each muscle control channel has its own Renshaw cell pool, which receives excitatory inputs from its channel's α-*MN* pool. The Renshaw pool sends inhibitory signals to its own channel's α-*MN* and *IaIN* pools, as well as to the opponent channel's Renshaw pool.

Consider the consequences of this signed connectivity under conditions of unequal recruitment. When P causes deeper recruitment in α-*MN* pool 1, the Renshaw population in channel 1 becomes much more active than in channel 2. This causes $\alpha\text{-}MN_1$ to be subjected to greater Renshaw inhibition than $\alpha\text{-}MN_2$, thus partially correcting channel 1's expected force advantage. Simultaneously, $\alpha\text{-}MN_2$ is disinhibited by two pathways:

$$R_1 \rightarrow R_2 \rightarrow \alpha\text{-}MN_2 \tag{10.26}$$

and

$$R_1 \rightarrow IaIN_1 \rightarrow \alpha\text{-}MN_2. \tag{10.27}$$

This further compensates for channel 1's expected force advantage by increasing the force developed by channel 2. Simulations reported by Bullock and Grossberg (1988b, 1989) showed that Renshaw-mediated compensation could virtually eliminate undesired joint rotations associated with variations in P for any given choice of (A_1, A_2). In our theory, then, Renshaw cells play a key role in ensuring the invariance principle formalized by equation (24).

The fully expanded FLETE model is shown in fig. 10.11 on page 282. This figure contains three more modifications to fig. 10.10D that we briefly touch on here. First, consideration of muscle fatigue and the imbalances it can introduce led to including Golgi tendon organs and *Ib* interneurons in the expanded FLETE model of fig. 10.11. Force feedback from the Golgi tendon organs to *Ib* interneurons compensates for muscle fatigue by inhibiting the α-*MN* in the same channel and the *IbIN* in the opposing channel; the addition of these pathways to the model has been shown through simulations to improve performance even without muscle fatigue.

Second, the realization that truly high performance of the motor control system cannot rely solely on the automatic, feedforward compensatory mechanisms described so far has led to the inclusion of error feedback mechanisms. This includes the well-known stretch reflex arc, consisting of γ motoneurons projecting to the intrafusal muscles, whose spindle organs in turn project to the α-*MN* and *IaIN*. Discrepancies between commanded muscle length at the γ-*MN* and actual length of the extrafusal muscles result in spindle organ excitation, which in turn results in α-*MN* excitation or inhibition to correct this discrepancy.

Third, consideration of changes in mechanical advantage of antagonistically paired muscles depending on joint angle has led to including a reconverging sideloop pathway, which incorporates error-driven learning into the command issued to the α-*MN*. Bullock and Grossberg (1990, 1991) follow in a tradition of work by Albus (1975), Ito (1984), Grossberg and Kuperstein (1986, 1989), and Kawato, Furukawa, and Suzuki (1987) by summarizing how such a central adaptive process sensitive to spindle feedback signals can learn an intended angle-dependent, preemptive compensation for angle-dependent variations in mechanical advantage. A key neural site for this and other instances of context-dependent adaptation of motor commands is the cerebellum, whose basic circuit we have begun to model at a level of detail similar to fig. 10.11 (see Bullock, Contreras-Vidal, and Grossberg 1993a; Contreras-Vidal 1994).

This completes the conceptual reconstruction of the peripheral neuromuscular system as a module that affords independent control of muscle length and joint stiffness. See Bullock and Contreras-Vidal (1993) for a summary of experimental evidence for all the cell types and connections (including sign) assumed in the model, as well as simulation results verifying the functionality we describe here. Since Bullock and Grossberg (1992), it has been known that variants of FLETE can also produce realistic transient muscle activations, such as the triphasic EMG pattern often observed during rapid, self-terminated movements (Lestienne 1979).

CONCLUDING REMARKS

This chapter has focused on the subset of neural network research concerned with explaining biological sensory-motor control. This approach seeks to explain detailed

psychophysical data on movement performance and identify neural substrates of the system components. Insights gained from psychophysics, anatomy, and physiology are formulated into models whose components derive from neural network and dynamical systems theory. This chapter has concentrated on a collection of interrelated neural networks, which form a system for performing the transformations from visually perceiving a target to specifying commands to the muscles that carry out a reach to the target. These networks resolve key problems in the theory of motor planning, inverse kinematics, and inverse dynamics. The VITE or DIRECT model can generate a kinematic trajectory with a uniphasic velocity profile, and therefore needs no preformed kinematic motor program. Similarly, the FLETE model can generate a multiphasic force profile, and therefore needs no preformed dynamic motor program. These networks highlight issues of autonomy, flexibility, and generativity in movement. They learn without an external teacher, optimize performance over a wide range of tasks, and automatically compensate for potential disruptions in movement performance. Many model cell types have been identified with *in vivo* neural populations that have similar operating characteristics and/or connectivity. We suspect that only through continued elaboration of such a model framework will there emerge a clear understanding of how the perceiving brain controls movement in animals.

REFERENCES

Albus, J.S. 1975. A new approach to manipulator control: The cerebellar model articulation controller (CMAC). *Transactions of the ASME Journal of Dynamic Systems, Measurement, and Control* 97 (September):220-227.

Barto, A.G. 1990. Connectionist learning for control. P. 5-58 in *Neural Networks for Control*, edited by W.T. Miller, III, R.S. Sutton, and P.J. Werbos. Cambridge, MA: MIT Press.

Bullock, D., and Contreras-Vidal, J.L. 1993. How spinal neural networks reduce discrepancies between motor intention and motor realization. P. 183-221 in *Variability and Motor Control*, edited by K.M. Newell and D.M. Corcos. Champaign, IL: Human Kinetics.

Bullock, D., Contreras-Vidal, J.L., and Grossberg, S. 1993a. Cerebellar learning in an opponent motor controller for adaptive load compensation and synergy formation. P. 481-486 in *Proceedings of the World Congress on Neural Networks, Portland, IV*. Hillsdale, NJ: Erlbaum.

Bullock, D., Contreras-Vidal, J.L., and Grossberg, S. 1993b. Equilibria and dynamics of a neural network model for opponent muscle control. P. 439-458 in *Neural Networks in Robotics*, edited by G. Bekey and K. Goldberg. Boston: Kluwer Academic.

Bullock, D., and Grossberg, S. 1988a. Neural dynamics of planned arm movements: Emergent invariants and speed-accuracy properties during trajectory formation. *Psychological Review* 95(1):49-90.

Bullock, D., and Grossberg, S. 1988b. Neuromuscular realization of planned trajectories. *Neural Networks* 1, Supplement 1:329.

Bullock, D., and Grossberg, S. 1989. VITE and FLETE: Neural modules for trajectory formation and tension control. P. 253-297 in *Volitional Action*, edited by W. Hershberger. Amsterdam: North-Holland.

Bullock, D., and Grossberg, S. 1990. Spinal network computations enable independent control of muscle length and joint compliance. P. 349-356 in *Advanced Neural Computers*, edited by R. Eckmiller. Amsterdam: Elsevier.

Bullock, D., and Grossberg, S. 1991. Adaptive neural networks for control of movement trajectories invariant under speed and force rescaling. *Human Movement Science* 10:1-51.

Bullock, D., and Grossberg, S. 1992. Emergence of tri-phasic muscle activation from the nonlinear interactions of central and spinal neural network circuits. *Human Movement Science* 11:157-167.

Bullock, D., Grossberg, S., and Guenther, F.H. 1993. A self-organizing neural model of motor equivalent reaching and tool use by a multijoint arm. *Journal of Cognitive Neuroscience* 5:408-435.

Bullock, D., Grossberg, S., and Mannes, C. 1993. A neural network model for cursive script production. *Biological Cybernetics* 70:15-28.

Busemeyer, J.R., and Townsend, J.T. 1993. Decision field theory: A dynamic-cognitive approach to decision making in an uncertain environment. *Psychological Review* 100:432-459.

Calabrese, R.L., Angstadt, J.D., and Arbas, E.A. 1989. A neural oscillator based on reciprocal inhibition. P. 33-50 in *Perspectives in Neural Systems and Behavior*, edited by T.J. Carew and D.B. Kelley. New York: Liss.

Carpenter, G.A., and Grossberg, S. 1987. A massively parallel architecture for a self-organizing neural pattern recognition machine. *Computer Vision, Graphics, and Image Processing* 37:54-115.

Cohen, M.A., Grossberg, S., and Pribe, C. 1993. A neural pattern generator that exhibits arousal-dependent human gait transitions. P. 285-288 in *Proceedings of the World Congress on Neural Networks, Portland, IV*. Hillsdale, NJ: Erlbaum.

Contreras-Vidal, J.L. 1994. Neural networks for motor learning and regulation of posture and movement. PhD diss. Boston University, Department of Cognitive and Neural Systems.

Cooke, J.D. 1980. The organization of simple, skilled movements. P. 199-212 in *Tutorials in Motor Behavior*, edited by G.E. Stelmach and J. Requin. Amsterdam: North-Holland.

DeJong, R., Coles, M.G.H., Logan, G.D., and Gratton, G. 1990. In search of the point of no return: The control of response processes. *Journal of Experimental Psychology: Human Perception and Performance* 16:164-182.

DeValois, R.L., and DeValois, K.K. 1975. Neural coding of color. In *Handbook of Perception. Vol. 5: Seeing*, edited by E.C. Carterette and M.P. Friedman. New York: Academic Press.

Feldman, A.G. 1986. Once more on the equilibrium-point hypothesis (λ model) for motor control. *Journal of Motor Behavior* 18:17-54.

Flash, T., and Hogan, N. 1985. The coordination of arm movements: An experimentally confirmed mathematical model. *Journal of Neuroscience* 5(7):1688-1703.

Foley, J.M. 1980. Binocular distance perception. *Psychological Review* 87:411-434.

Gaudiano, P., and Grossberg, S. 1991. Vector associative maps: Unsupervised real-time error-based learning and control of movement trajectories. *Neural Networks* 4:147-183.

Georgopoulos, A.P., Kalaska, J.F., Caminiti, R., and Massey, J.T. 1982. On the relations between the direction of two-dimensional arm movements and cell discharge in primate motor cortex. *Journal of Neuroscience* 2:1527-1537.

Greve, D., Grossberg, S., Guenther, F.H., and Bullock, D. 1993. Neural representations for sensory-motor control, I: Head-centered 3-d target positions from opponent eye commands. *Acta Psychologica* 82:115-138.

Grossberg, S. 1968. Some nonlinear networks capable of learning a spatial pattern of arbitrary complexity. *Proceedings of the National Academy of Sciences* 59(2):368-372.

Grossberg, S. 1973. Contour enhancement, short-term memory, and constancies in reverberating neural networks. *Studies in Applied Mathematics* 52:217-257.

Grossberg, S. 1982. *Studies of Mind and Brain.* Dordrecht, Holland: Reidel.

Grossberg, S., Guenther, F., Bullock, D., and Greve, D. 1993. Neural representations for sensory-motor control, II: Learning a head-centered visuomotor representation of 3-d target positions. *Neural Networks* 6:43-67.

Grossberg, S., and Kuperstein, M. 1986. *Neural Dynamics of Adaptive Sensory-Motor Control: Ballistic Eye Movements.* Amsterdam: North-Holland.

Grossberg, S., and Kuperstein, M. 1989. *Neural Dynamics of Adaptive Sensory-Motor Control, Expanded Edition.* Elmsford, NY: Pergamon Press.

Guenther, F.H. 1992. *Neural Models of Adaptive Sensory-Motor Control for Flexible Reaching and Speaking.* PhD diss., Boston University, Department of Cognitive and Neural Systems.

Guenther, F.H. 1994. A neural network model of speech acquisition and motor equivalent speech production. *Biological Cybernetics* 72:43-53.

Guenther, F.H., Bullock, D., Greve, D., and Grossberg, S. 1994. Neural representations for sensory-motor control, III: Learning a body-centered representation of 3-d target position. *Journal of Cognitive Neuroscience* 6:341-358.

Henneman, E. 1957. Relation between size of neurons and their susceptibility to discharge. *Science* 26:1345-1347.

Houk, J.C., and Gibson, A.R. 1987. Sensorimotor processing through the cerebellum. P. 387-416 in *New Concepts in Cerebellar Neurobiology*, edited by J.S. King. New York: Liss.

Humphrey, D.R., and Reed, D.J. 1983. Separate cortical systems for control of joint movement and joint stiffness: Reciprocal activation and coactivation of antagonist muscles. P. 347-372 in *Motor Control Mechanisms in Health and Disease*, edited by J.E. Desmedt. New York: Raven Press.

Ito, M. 1984. *The Cerebellum and Neural Control.* New York: Raven Press.

Jordan, M. 1988. Supervised learning and systems with excess degrees of freedom. Technical Report COINS 88-27, Computer and Information Sciences, University of Massachusetts at Amherst, MA.

Kalaska, J.F., Cohen, D.A.D., Hyde, M.L., and Prud'homme, M. 1989. A comparison of movement direction-related versus load direction-related activity in primate cortex, using a two-dimensional reaching task. *Journal of Neuroscience* 9(6): 2080-2102.

Kawato, M., Furukawa, K., and Suzuki, R. 1987. A heirarchical neural-network model for control and learning of voluntary movement. *Biological Cybernetics* 57:169-185.

Kohonen, T. 1984. *Self-Organization and Associative Memory.* New York: Springer-Verlag.

Kuperstein, M. 1988. An adaptive neural model for mapping invariant target position. *Behavioral Neuroscience* 102(1):148-162.

Lacquaniti, F., Soechting, J.F., and Terzuolo, C.A. 1982. Some factors pertinent to the organization and control of arm movements. *Brain Research* 252:394-397.

Lestienne, F. 1979. Effects of inertial load and velocity on the braking process of voluntary limb movements. *Experimental Brain Research* 35:407-418.

Levine, D.S. 1991. *Introduction to Neural and Cognitive Modeling.* Hillsdale, NJ: Erlbaum.

Masino, T., and Knudsen, E.I. 1990. Horizontal and vertical components of head movement are controlled by distinct neural circuits in the barn owl. *Nature* 345:434-437.

McClelland, J.L., and Rumelhart, D.E. 1981. An interactive activation model of context effects in letter perception: Part 1. Account of basic findings. *Psychological Review* 88(5):375-406.

Merton, P.A. 1972. How we control the contraction of our muscles. *Scientific American* 226:30-37.

Miller, W.T. III. 1987. Sensor-based control of robotic manipulators using a general learning algorithm. *IEEE Journal of Robotics and Automation* RA-3(2):157-165.

Mollon, J.D., and Sharpe, L.T. 1983. *Colour Vision.* New York: Academic Press.

Morasso, P. 1981. Spatial control of arm movements. *Experimental Brain Research* 42:223-227.

Nagasaki, H. 1989. Asymmetric velocity and acceleration profiles of human arm movements. *Experimental Brain Research* 74:319-326.

Narendra, K.S. 1990. Adaptive control using neural networks. P. 115-142 in *Neural Networks for Control*, edited by W.T. Miller III, R.S. Sutton, and P.J. Werbos. Cambridge, MA: MIT Press.

Piaget, J. 1963. *The Origins of Intelligence in Children.* New York: Norton.

Polit, A., and Bizzi, E. 1979. Characteristics of motor programs underlying arm movements in monkeys. *Journal of Neurophysiology* 42:183-194.

Rack, P.H.M., and Westbury, D.R. 1969. The effect of length and stimulus rate on the tension in the isometric cat soleus muscle. *Journal of Physiology* 204:443-460.

Raibert, M.H. 1977. Motor control and learning by the state space model. Technical Report AI-M-351, Massachusetts Institute of Technology. NTIS AD-A026-960.

Ritter, H.J., Martinetz, T.M., and Schulten, K.J. 1989. Topology-conserving maps for learning visuo-motor-coordination. *Neural Networks* 2:159-168.

Selverston, A.I., and Moulins, M., eds. 1986. *The Crustacean Stomatogastric System.* New York: Springer-Verlag.

Uno, Y., Kawato, M., and Suzuki, R. 1987. Formation of optimum trajectory in control of arm movement: Minimum torque-change model. Technical report, Japan IEICE.

Vidal, P.P., de Waele, C., Graf, W., and Berthoz, A. 1988. Skeletal geometry underlying head movements. P. 228-238 in *Representation of Three-Dimensional Space in the Vestibular, Oculomotor, and Visual Systems*, Volume 545 of *Annals of the New York Academy of Sciences*, edited by B. Cohen and V. Henn. New York: New York Academy of Sciences.

von der Malsburg, C. 1973. Self-organization of orientation sensitive cells in the striate cortex. *Kybernetik* 14:85-100.

Zelaznik, H.N., Schmidt, R.A., and Gielen, C.C.A.M. 1986. Kinematic properties of rapid aimed hand movements. *Journal of Motor Behavior* 18:353-372.

Zipser, D., and Andersen, R.A. 1988. A back-propagation programmed network that simulates response properties of a subset of posterior parietal neurons. *Nature* 331:679-684.

Appendix

Modeling Neural Networks as Dynamical Systems

Neural networks are ubiquitous in animals and form the basis of natural intelligence. Since the time of the pioneering neurobiologists Cajal and Sherrington, we have known these networks are composed of excitable cells called neurons, which often communicate with other neurons across physical discontinuities known as synapses. To describe neurons as excitable is to say that they are active elements, and that the fluctuations in their *activation level* are at least partly dependent on inputs, whether from other cells or from outside the network. We also know that the *efficacy* of trans-synaptic communication between some kinds of cells changes, again at least partly dependent on inputs. We can think of both neural activation level and synaptic efficacy as continuous variables of the neural network.

To understand how activation patterns and synaptic efficacies within these networks can evolve and generate intelligent behavior, it is necessary to describe the biophysical laws governing both types of variables. A mathematical rule describing a lawful relation between some dependent variable and factors that cause continuous changes in that dependent variable is a *differential equation*. Thus, differential equations provide the natural language for describing neural networks. If we can use a differential equation to describe all the important factors that determine changes in a dependent variable, and if we can determine the value of that variable at some initial time and know the time histories of the controlling factors after that initial time, then we can compute the time history of the dependent variable for all subsequent times. Performing such a computation is known as solving an *initial value problem*: we start the dependent variable at its initial value, then compute its changes under the influence of the determining factors. If we want to track the evolution, or time history, of many variables (e.g., the activation levels of many cells in a neural network), then we need a differential equation for each distinct cell, and we will have to solve the initial value problem for an entire system of differential

equations. Such systems of differential equations are known as dynamical systems, a term often used to refer to the natural systems described or modeled by systems of differential equations.

An inherent characteristic of neural networks is that the cells in a network communicate with one another. Each cell's activation level can therefore be a determining factor for other cells. In such cases, we do not know the time histories of the controlling factors in advance. All the cellular activation levels, and their determining factors, which include other cells' activation levels, are evolving at once. Can we still solve the initial value problem? The answer is yes, but accurate solution requires that we continuously and simultaneously update each cell's set of determining factors as time proceeds. It will not suffice to trace one cell's entire time history, then the next cell's, and so forth. This would represent a serial evolution, not the parallel, simultaneous evolution characteristic of neural networks. With a serial, digital computer, the best we can do is to approximate continuous and simultaneous updating of all cell activation levels. We do this by slicing time into very small steps, and letting the determining factors act on each (simulated) cell for only a brief time before updating the next cell. Though this is a serial process, it is virtually parallel, because all cells are updated within so short a time that updating is almost simultaneous. Methods that do such updating by computer are known as numerical methods for solution of differential equations. Because such methods add up, or integrate, the net effect of all the changes to a variable through time, they are also called numerical integration routines. These methods range from fast, simple, but error-prone routines, such as Euler's simple method, to more sophisticated, less error-prone, but slower methods, such as Euler's improved method, the Runge-Kutta method, and Gear's method.

One of the most desirable properties of differential equation modeling is the natural way it allows us to represent the idea that the time it takes for a dependent variable to evolve from some initial value to some final value depends on the net strength of the determining factors pushing the dependent variable from the initial value toward the final value. As an example, consider the following facts about between-neuron communications and neuronal activation dynamics. When one cell releases an excitatory transmitter into a synapse, this transmitter diffuses across to the adjacent cell, where it opens gates in the target cell's membrane. This allows an increased flow, or current, of certain ions into the target cell, a physical process that takes time. The amount of transmitter determines how many gates open and therefore the upper bound on flow per unit time, the flow rate. The total amount of flow determines how much the target cell's activation is raised above its initial value, and the rate of flow determines how quickly this net change occurs. In real cells, the ionic flow will always stop when the cell reaches an inherent upper bound on its activation level, and the flow slows as the cell approaches this upper bound, even if a large amount of excitatory transmitter is bombarding the cell's membrane. These properties are captured by the following differential equation:

$$dX/dt = (B - X)I \tag{A1}$$

where X is the cell's activation level, B is the fixed upper bound on the cell's activation level, and I is the amount of excitatory transmitter (more precisely, the

net conductance, or openness to current flow, of the gates affected by the transmitter). This equation tells us that the instantaneous rate, dX/dt, at which the neuron's activation level X can be driven from an initial value of 0.0 toward activation level B is partly determined by the amount, I, of excitatory transmitter. More transmitter will reduce the time needed for the neuron to go from 0 to B, just as more gas will reduce the time needed for a car to go from 0 to 200 kph. The equation also tells us that once X becomes equal to B, the rate, dX/dt, at which the neuron gains activation becomes zero, because then $B - X = 0$, and $dX/dt = 0 \times I = 0$, however large the value of I. Thus, the equation captures the properties of neuronal activation dynamics described previously.

Extensions of these elementary ideas have led to systematic treatment of many rate-dependent behavioral phenomena, such as voluntary control of movement speed and speed-accuracy tradeoffs (Bullock and Grossberg 1988a; 1991), control of gait transitions in locomotion (Cohen, Grossberg, and Pribe 1993), and control of learning rate (Carpenter and Grossberg 1987).

Acknowledgments

Daniel Bullock is supported in part by the National Science Foundation (NSF IRI 90-24877 and NSF IRI 87-16960) and the Office of Naval Research (ONR N00014-92-J-1309).

Stephen Grossberg is supported in part by the Air Force Office of Scientific Research (AFOSR F49620-92-J-0499), the National Science Foundation (NSF IRI 90-24877 and NSF IRI 87-16960), and the Office of Naval Research (ONR N00014-92-J-1309).

Frank Guenther is supported in part by the National Science Foundation (NSF IRI 90-24877 and NSF IRI 87-16960) and the Air Force Office of Scientific Research (AFOSR F49620-92-J-0499).

Credits

Figure 5.2 Reprinted, by permission, from L.S. Jakobson and M.A. Goodale, 1991, "Factors influencing higher-order movement planning: A kinematic analysis of human prehension," *Experimental Brain Research* 86.

Figure 5.3 Reprinted, by permission, from L.S. Jakobson and M.A. Goodale, 1991, "Factors influencing higher-order movement planning: A kinematic analysis of human prehension," *Experimental Brain Research* 86.

Figure 5.4 Reprinted, by permission, from L.S. Jakobson and M.A. Goodale, 1991, "Factors influencing higher-order movement planning: A kinematic analysis of human prehension," *Experimental Brain Research* 86.

Figure 5.5 Reprinted from *Vision Research*, vol. 32, P. Servos, M.A. Goodale, and L.S. Jakobson, The role of binocular vision in prehension: A kinematic analysis, Copyright 1992, with kind permission of Pergamon Press Ltd, Headington Hill Hall, Oxford, OX3 0BW, United Kingdom.

Figure 5.6 Reprinted from *Vision Research*, vol. 32, P. Servos, M.A. Goodale, and L.S. Jakobson, The role of binocular vision in prehension: A kinematic analysis, Copyright 1992, with kind permission of Pergamon Press Ltd, Headington Hill Hall, Oxford, OX3 0BW, United Kingdom.

Figure 5.7 Reprinted from *Vision Research*, vol. 32, P. Servos, M.A. Goodale, and L.S. Jakobson, The role of binocular vision in prehension: A kinematic analysis, Copyright 1992, with kind permission of Pergamon Press Ltd, Headington Hill Hall, Oxford, OX3 0BW, United Kingdom.

Figure 5.8 Reprinted, by permission, from L.S. Jakobson and M.A. Goodale, 1991, "Factors influencing higher-order movement planning: A kinematic analysis of human prehension," *Experimental Brain Research* 86.

Figure 5.9 Reprinted, by permission, from P. Servos and M.A. Goodale, 1994, "Binocular vision and the on-line control of human prehension," *Experimental Brain Research* 98: 119-127.

Figure 5.10 Reprinted, by permission, from P. Servos and M.A. Goodale, 1994, "Binocular vision and the on-line control of human prehension," *Experimental Brain Research* 98: 119-127.

Figure 5.11 Reprinted, by permission, from P. Servos and M.A. Goodale, 1994, "Binocular vision and the on-line control of human prehension," *Experimental Brain Research* 98: 119-127.

Figure 5.12 Reprinted, by permission, from Mishkin et al., 1983, "Object vision and vision: Two cortical pathways," *Trends in Neuroscience* 6.

Figure 5.13 Reprinted by permission for *Nature* vol. 349, pp. 154-156; Copyright 1991 Macmillan Magazines Limited.